AFM investigation of mechanical properties of dentin

"AFM Investigation of mechanical properties of dentin"

Sidney R. Cohen*, Nathan Apter
Department of Chemical Research Support, Weizmann Institute of Science, Rehovot ISRAEL 76100

Stephen Jesse, Sergei Kalinin
Oak Ridge National Laboratory, Center for Nanophase Materials Research

David Barlam
Ben Gurion University of the Negev

Adi Idit Peretz, Daniel Ziskind, and H. Daniel Wagner
Department of Materials and Interfaces, Weizmann Institute of Science, Rehovot ISRAEL 76100

ABSTRACT. Mechanical properties of peritubular dentin were investigated using scanning probe microscopy techniques, namely Nanoindentation and Band Excitation. Particular attention was directed to the possible existence of a gradient in these properties moving outward from the tubular lumen to the junction with the intertubular dentin. Finite element analysis showed that the influence of the boundaries is small relative to the effects observed. Thus, these results strongly support the concept of a lowering of modulus and hardness from the tubular exterior to its periphery, which appear to correlate with graded changes in the mineral content.

*Corresponding author. Email: Sidney.cohen@weizmann.ac.il

INTRODUCTION

Knowledge of the mechanical properties of dentin is the first critical step in understanding how masticatory strains are distributed throughout the tooth, and eventually could help predict how stresses and strains are altered by dental restorative procedure, age and disease.[1] It is also necessary to gain insight into caries, sclerosis, ageing, cracked tooth syndrome, and the effects of the wide variety of restorative dental procedures that range from preparation design to bonding protocols. Moreover, these insights can be applied to improve the quality and performance of synthetic composite materials used in dentistry, and even to gain a basic understanding of the mechanics of general composite materials. Hence, for many years great effort has been invested in understanding the mechanical behaviour of dentin.

Structurally, dentin can be viewed in two hierarchical levels (see Fig. 1): An intricate hydrated biological micro-composite with highly oriented tubule-like structures embedded in a mineralized collagen-rich matrix called intertubular dentin (ITD), and the basic structural building block presenting unique orientation and variable modes of crystal dimension. The "tubules" diverge from the pulp to the enamel. Such a tubule consists of a lumen (inner, hollow core) surrounded by a hypermineralized collar called Peritubular dentin (PTD). Each tubule is formed by an elongated odontoblastic process creating a sinuous path organization. The network of the mineralized collagen fibrils forms the basic structural building block of the dentin presenting unique orientation and variable modes of crystal dimension and organization.[2] Depending on location a single dentinal tubule is 1 μm to 2.5 μm in diameter.

Critically reviewed research of the past 50 years indicated that the magnitudes of the elastic constants of dentin must be revised considerably.[3] For example, the reported values of Young's modulus of dentin span a range from approximately 10 to over 40 GPa. [3, 4, 5, 6, 7] The experimental methodologies for many years concentrated on bulk dentin compression and microhardness testing, thus the measured properties averaged over the various microstrucutres. Young's modulus, tensile and compressive strength, and fracture toughness may be influenced by the material structure at the submicron scale. Thus tubule density and orientation, as well as collagen fiber direction and the local average density of the mineral phase all contribute to the mechanical behavior.

Hardness and elastic modulus are two key parameters by which materials strength is defined. Determination of hardness and elastic modulus from depth-sensing indentation instruments, based on the work of Doerner and Nix was for years the classic means for defining these properties at a specific sample location.[8] In 1992, Oliver and Pharr introduced an improved method for determining values of hardness and elastic modulus from indentation experiments.[9, 10] In the past decade, such measurements have been successfully extended down to the nanoscale by limiting indentation depths to several tens of nm, corresponding to applied loads in the range of tens to hundreds of microNewtons.

Application of AFM to studies of nanomechanics was proposed shortly after its invention, with the demonstration of semi-quantitative measurements of the local modulus.[11] Systematic application of scanning probe techniques to investigate local mechanical properties has developed much more slowly for several reasons. One is the dynamic range: whereas a nanoindenter applies a calibrated force, variable over several orders of magnitude, and measures displacement, in AFM we control the displacement only. The force applied is related to displacement by Hooke's law and the cantilever spring constant. Typical cantilever spring constants used in contact imaging - around 1 N/m or less - are not useful for probing surfaces with moduli greater than some tens of MPa because the contact stiffness $S=2aE^*$ (a = contact radius and E^* effective modulus) greatly exceeds the cantilever spring constant. Consequently, the deformation would occur nearly exclusively in the cantilever, not the sample. In order to accurately measure surfaces with moduli of several GPa or more such as dentin, using a tip of radius around 20 nm, a spring constant of hundreds of N/m is needed.[12] The resulting high scanning forces could easily damage sample or tip. The tip shape itself presents another problem, as the common sharp silicon or silicon nitride probes used in AFM do not have a regular geometrical shape, complicating quantitative analysis. Additionally, the cantilever geometry does not provide the rigidity of the indenter in a dedicated nanoindenter, and is subject to lateral motions which could give rise to spurious signals.[13]

These compliance problems can be overcome by: (1) using very stiff cantilevers with diamond tips, whereby surface topography is measured using noncontact or intermittent contact imaging, and (2) coupling the vertical tip-surface motion with a lateral motion during the indentation which nullifies the predicted lateral deflections.

In addition to indentation techniques based on evaluation of quasistatic force/displacement curves, some SPM techniques exist which evaluate the surface mechanical properties by monitoring the dynamics of the driven cantilever motion as the tip interacts with the surface. Vertical modulation of the sample surface during scanning was first applied to a polymer composite, providing surface mapping with quantitative estimate of the modulus.[14] When vibration frequency is raised to ultrasonic frequencies to access higher contact frequencies, the effective cantilever stiffness is raised, allowing mapping of surface elasticity even with relatively soft cantilevers.[15], [16] These techniques address some of the problematic aspects of AFM-based nanoindentation. One is the dynamic range, in that a wide range of surface compliances can be measured with one cantilever. Furthermore, the frequency-sensitive detection enhances sensitivity so that finer variations of the modulus with shallower indentation depths are achieved. Finally, since the excitation can be mechanical or electromechanical, piezoresponse can be monitored simultaneously with the pure mechanical response. For biological samples such as dentin, this allows some material differentiation since collagen has a piezoelectric response, whereas the mineral parts do not so that mineral vs. organic collagen content of the dentin can be correlated with the electromechanical and mechanical behaviour.[17], [18] These methods are still under development and require a good deal of finesse. The inertial stiffening obtained at frequencies above the first cantilever resonance indeed allow probing a larger range of materials, but when the amplitudes rise above a threshold level, the cantilever motion becomes chaotic so that quantitative results can no longer be had.[19] Furthermore, separating topographical and mechanical effects is not always possible.[20]

Band Excitation (BE) is a new technique whereby a full response spectrum is measured over a grid of points across the sample surface.[21] The system can be excited by a bias signal applied between sample and tip, or by a pure mechanical excitation of the sample. In BE, at each measurement point, a continuous band of frequencies around a resonance is excited and recorded. The resulting response to this excitation is Fourier transformed to give the resonance peak shape from which various dynamic parameters such as resonance frequency, amplitude at resonance, and Q, are obtained. The resonance frequency can be directly related to the modulus, Q to the dissipation and amplitude to piezoresponse in the case of electromechanical excitation. By

designing an excitation frequency pulse that maximizes the trade-off between signal-to-noise and frequency resolution in the frequency range of interest, rapid data acquisition is achieved. This technique is superior to those where the response is measured at a single frequency, in which case the single harmonic oscillator equation cannot be uniquely defined and hence power dissipation which occurs due to inhomogeneities in the local force cannot be clearly separated from the overall dynamics.

Clearly, application of these high-resolution techniques to examine dentin properties on the micro-scale is appealing. By using AFM mappings of the region to guide indentation placement, it is possible to evaluate the hardness and Young's modulus as a function of distance from the hollow tubular core (lumen) across the PTD which comprises the tubular cross-section, until and across the PTD-ITD junction (PIJ). In addition, evaluation of the PTD and the ITD separately facilitates assessment of whether the changes in dentin modulus and hardness are due to the morphology, or to the changing mineral composition at a specific location in the dentin [22] A higher piezoresponse in the ITD has been associated with enhanced collagen content relative to the largely mineralized PTD. [23] AFM-based nanoscratching has also been used to estimate the fine mechanical changes across a dental boundary.[24]

The fine resolution lent by these techniques opens the opportunity to investigate the interesting problem of material and mechanical variations within the PTD. Using a modulation technique, Balooch et al analyzed the width of the PIJ and found a slight gradient across and adjacent to the PIJ. The width of the PIJ was carefully analyzed and found to be approximately half of the PTD width (FWHM 0.3 vs. 0.7 functional width).[5] However, this work did not address the possibility of a gradient of mechanical properties across the entire PTD. Indeed, variations in the mechanical properties across the PTD were associated with the effect of the PIJ and lumen.[25]

These studies show the critical role of the "edge effect: When making nanomechanical measurements at high spatial resolution, edge effects must be considered. Since the volume of the stress field extends significantly beyond the deformed volume, influence of neighboring regions must be considered.[26]As a rule of thumb, mechanical response will be influenced by material phases at vertical depths up to ten times the depth of the indentation, and lateral phases or interfaces at distances up to several times the cross-section of the indentation. For this reason, it is

important to make the force measurement with the minimal depth required to avoid bias due to surface morphological irregularities.

This work exploits the strengths of the AFM - The low inertia, and high frequencies achievable allow superior imaging and positioning. Furthermore, AFM provides imaging modes, such as intermittent-contact, which can yield quality images of delicate samples which would be damaged under contact-mode scanning with an indenter tip. By performing AFM-based quasi-static and BE measurements across the PTD, a true variation of mechanical properties was observed, unrelated to the proximity of the PIJ. Comparison to Finite Element Analysis simulations is provided to visualize the lateral extent of the stress field and deduce the relative influence of the edge effect.

Experimental

After embedding the tooth in epoxy resin (Epofix®, Struers, Copenhagen, Denmark), a slice of crown dentin was isolated by cutting off the enamel and pulp chamber using a water cooled diamond saw (Minitom® Struers, Copenhagen, Denmark). (Figure 1). Thereafter, the pulpal aspects of each slice were metallographically ground through a series of SiC abrasive papers and polished using diamond suspensions of 9.0 and 1.0 μm particle size, on soft polishing cloths (LaboForce-3® & LaboPol-2®, Struers, Copenhagen, Denmark). The samples were rinsed copiously under water and cleaned ultrasonically after each polishing step.

AFM imaging and quasi-static indentation tests were performed using an NTEGRA AFM (SU005 head, NT-MDT, Russia). The probe used was a cube-corner diamond tip metal bonded on a sapphire cantilever [Microstar Tech., Huntsville, CA U.S.A]. Several probes were applied, with cantilever force constants ranged from 300 – 900 N/m, with resonant frequencies in the range of 60 – 120 kHz. The height of the diamond tip ranged from tens, up to over 100 microns.

Imaging was performed in intermittent-contact mode at a scan rate of less than 1 Hz per line over frame sizes less than 5x5 μm^2, to avoid damage to the sharp tip when

entering the deep lumen structure of the tubule. A closed-loop system was used to accurately position the indentation from this acquired image, and images performed after the indentations were used to analyze the residual indentation area.

A custom software script controlled the experiment. Each indentation comprised three segments: loading, holding time and unloading. A force- displacement curve was obtained for each cycle of indentation (Fig. 2). The unloading phase is assumed to involve only elastic recovery. Before each such indentation cycle, the tip was positioned over the desired location while still operating in the semicontact (intermittent-contact) mode, then the modulation was disabled and the indentation process began, guided by preset indentation parameters (rate, lateral correction angle, and maximum load). Cantilever deflection past a set threshold defined the first contact with surface.

BE measurements were made with a MMAFM AFM head (Veeco, Santa Barbara CA) controlled by a Nanonis controller (Nanonis, Zurich, Switzerland). The excitation was driven by either bias applied between tip holder and bottom of sample, or by an ultrasonic transducer to which the sample was glued. For electrical excitation, either Olympus AC240 probes with nominal spring constant of 2 N/m were used in contact mode (first contact resonance between 350 – 400 kHz) or platinum-coated PPT (Nanosensors, Germany) tips with first contact resonance between 60 – 80 kHz. A custom Labview program (National Instruments Austin, TX) controlled the BE experiment, providing the appropriate waveform applied at each point of a grid selected on the image and applying a fitting routine to yield the SHO parameters offline.

Prior to each experiment calibrations were performed for cantilever sensitivity and for approach angle. Cantilever sensitivity was checked by pressing the tip against a hard sapphire substrate and monitoring deflection vs. displacement. The cantilever is affixed at an angle of 13 degrees with respect to the sample plane. When the tip is pushed against the sample with pure vertical motion, this angle leads to the generation of a lateral force at the tip, and consequential bending of the cantilever due to torque generated at the tip-sample contact. This bending is indistinguishable from that caused by a purely normal force at the photodiode detector. To counter this effect, the lateral force must be compensated by an opposing motion of the sample in contact with the tip. This is accounted for by moving the sample in Z and Y directions simultaneously

during loading and unloading, nullifying this lateral motion. The correction angle was determined empirically by performing a series of indentations on fused silica with angles ranging from 0^o (no correction) to 65^o - y movement of δzsin(65) at a force limit of approximately 100 μN. The correction angle was determined as that for which the pile-up around the indentation footprint was evenly distributed to all sides, Fig. 3.

Young's modulus calculations relied on the unloading segment according to the protocol developed by Oliver and Pharr.[9] The hardness was calculated in the traditional manner by dividing the maximum force, F_{max}, by the projected contact area, A_c, determined from the residual impression.

$$H = \frac{F_{\max}}{A_c} \qquad \textbf{Eq. 1}$$

The stiffness, S=dN/dz, was determined from the slope of the initial portion of the unloading curve (20%), using a linear fit. The reduced Young's modulus, E^*, was calculated from the measured stiffness, S, and Ac

$$E^* = \beta \cdot S \frac{\sqrt{\pi}}{2\sqrt{A_c}} \qquad \textbf{Eq. 2}$$

where β is a factor depending on the indenter geometry, where β≈ 1.034 for a 3-sided pyramidal indenter.

The effect on the reduced Young's modulus, E^*caused by deformations in the diamond indenter have an insignificant (< 3%) effect on the results.

The reduced Young's modulus E* is related to E by the relation $E^* = \frac{E}{1-\nu^2}$. The Poisson ratio in the PTD, ν_{PTD}, can be approximated according to the rule of mixtures, expressed as follows:

$$\nu_{PTD} = V^f_{apatite} \cdot \nu_{apatite} + V^f_{collagen} \cdot \nu_{collagen} \qquad \textbf{Eq. 3}$$

where ν is the Poisson ration, V^f is the volume fraction of the peritubular dentin (PTD), mineralized carbonated hydroxapatite (apatite), and collagen fibrils.

From published $\nu_{apatite}$ and $\nu_{collagen}$ values (0.28 and 0.35, respectively) [27] and considering the PTD is approximately 90% mineral, the value for ν_{PTD} was calculated

to be 0.29. Considering the effect of changing mineral content across the PTD, we note that for 70% mineral content, this value rises to 0.3 which would have a negligible (< 1%) effect on E. Contact area under load is determined using Eq. 2, with area as function of depth determined by indentations on fused silica with known modulus of 72 GPa. Since this gives the area under load, it may differ from the classic definition based on area from residual hardness impression. This has been shown to be an unimportant distinction unless E is much smaller than H, which is not the case here (vide infra).[28] For hardness measurements the contact area is evaluated directly from the AFM image using grain analysis by defining the indentation footprint as a pore.

Finite Element Analysis was performed using the MSC.MARC software package. The sample was modeled as a hollow tubule embedded in an infinite matrix. The boundary between the tube and matrix is seamless. The indenter tip was a rigid Berkovich geometry. The condition of contact between the tubule surface and indenter is defined. Part of the Finite Element Model (FEM) is shown in Fig. 4. Both the inner and the outer regions representing PTD and ITD respectively were built from hexahedral elements. The problem comprises 11800 such hexahedral elements. Total downward motion of indenter, corresponding to sample deformation was 50 nm, calculated in 50 concurrent increments. This is appropriate for comparison with experimental indents of 70-80 nm where surface roughness is 20-30 nm peak-to-peak.

In order to explore the effect of nearby phases with different moduli, the PTD was assigned a modulus of 35 GPa and the ITD a modulus of 15 GPa. The tubule is assigned an overall diameter of 3.5 microns, with a 1 micron hole in the center. 5 indentations were placed 0.2, 0.4, 0.6, 0.8 and 1 micron from the PTD-ITD junction. Poisson ratio was taken as 0.28 for both phases. Data for deformation as function of load are calculated, and these are converted to modulus using the area function of a Berkovitch tip and Eq. (2). Results are normalized to an identical simulation carried out on an infinite flat of modulus 35 GPa.

Results and Discussion

AFM nanoindentations were made on the crown dentin sample which was cut to expose the PTD cross-section perpendicular to the long axis. Quasi-static

indentations were spaced by 300- 400 nm in order to allow several indentations to be placed within the PTD without overlap of the footprints.

Determination of the area function using the fused silica standard proved unsatisfactory. Since the modulus of fused silica is several times larger than that of dentin, the dynamic range of the cantilevers appropriate for the latter were not optimal for achieving comparable depths in the standard. Limiting forces ranging between 50 μN to 135 μN were applied to generate different indentation depths of 10-25 nm. These depths were not sufficient to generate a useful calibration curve. Hence, the imaging function of the AFM was used to measure A_c directly from the residual indented area. This value was used for the calculation of hardness. The traditionally used parameter is a practical term, which does not rely on models describing the intricacies of the actual contact area and tip shape. Still, it can be used for direct quantitative comparison between the different locations, and even with other works. Furthermore, hardness values can be related to the elastic modulus in a simple form.[29]

Fig.5 shows an AFM image of a region including tubular lumen, PTD, and neighboring ITD. The PTD shows as a bright-contrast ring around the lumen. The footprints observed are from four sets of indentations extending radially across the PTD and across the PTD-ITD junction. A dramatic increase in this area with distance from the lumen is evident for the tests, made at 3 different maximum loads. This can be correlated to a decrease in the hardness and consequently the Young's modulus values with distance from the tubule lumen. The average hardness values measured for positions within the PTD which are either closer to the lumen edge, or to the PIJ, and also in the ITD are given in Table 1. The clear gradient in hardness values was observed for PTD located near the pulp. Interestingly, this gradient did not exist for PTD located near the Dentin-Enamel Junction. The gradient in the hardness values agrees with material variations indicated by electron microscopy work.[30]

Figure 6 depicts BE amplitude, phase, and Q mappings together with the AFM topography image. The sample was root dentin, and the tubule oriented with the long axis of the tubule nearly parallel to the sample surface, so that the depression in the topography image exposes the boundary of the lumen at its bottom, with the cross section of the PTD extending above it. The boundaries of the rectangular measurement grid are shown by the black box and define the array of the BE measurements. Thus, the bottom center of the BE plots represents the inner edge of

the PTD, with the cross-section of the PTD extending as an annular ring above this. The results clearly indicate a maximum in the resonance frequency (Fig. 6(a), bright contrast) at the inner part of the tubule closest to the lumen which is the bottom central part of figure. This corresponds to a maximum in the modulus. Moving outwards across the PTD toward the PTD-ITD junction, the contrast gets darker, indicating a decrease in the modulus. This result corresponds well to the results of the quasi-static indentations. The extent and influence of dissipation must be taken into consideration when comparing quasi-static measurements, made at frequencies near 1 Hz, with dynamic measurements made at frequencies 5 orders of magnitude or more higher than this. The Q - dissipation - mapping, of Fig. 6(b) shows that dissipation varies inversely to modulus so that the regions nearest the lumen have lower dissipation relative both to the PTD closer to the ITD and the ITD itself. Finally, the amplitude images of Fig. 6(c) delineate changes in the piezoelectricity, since excitation was induced electromechanically. The observed contrast displays no detectable piezoresponse on the inner part of the PTD, with a growing amplitude near the PIJ. Whereas some of the contrast here correlates with topography, the effect is clearly not due to changing tip/surface contact area across the image: Only about 1/3 of the images showed the trend depicted here for the three signals. The other images showed no decisive and consistent change of properties over the cross-section. This is likely due to surface effects: since BE involves very shallow penetration into the surface, it is very sensitive to surface contaminants and irregularities which could arise during the preparation. For this reason, independent verification of models and other experiments provide valuable confirmation of the results. The outstanding features of the BE are the sensitivity and resolution which are unobtainable by other techniques. Furthermore, the amplitude (piezoresponse) signal provides a materials contrast since it correlates with the collagen content and inversely with the mineral content.

Results of the FEA simulations are shown in Table 2. The simulation was run to a depth of 50 nm. Since the model surface is perfectly flat, this roughly corresponds to a real surface with p-p roughness of 20-30 nm and real experimental indentation depth of 70-80 nm, similar to that used in the AFM nanoindentations. There are two boundary effects in the PTD, that of the empty volume at the lumen, and that of the PTD-ITD junction. These simulations were designed to check the boundary effect of

the hollow lumen on one side, and the ITD on the other. The distribution of normal stress is shown in figure 7 for an indentation 0.6 microns from the lumen. Clearly the stress distribution falls significantly (several orders of magnitude fall-off within the plotted volume which confined to a region distant from the PTD boundaries. This is true for all but the extreme indentations. The largest effect is seen at the indent closest to the lumen, with modulus of 26.7 GPa. The modulus rises significantly when the indentation is moved by 200 nm further from the hollow lumen. The remainder of the indentations show a very modest variation, less than 3%. Thus, experimental values showing changes by a factor of 2 in hardness must represent a real gradient in the local material property and not an effect due to proximity of one of the boundaries. The low value near the lumen is likely related to the idealized model used, with the hollow of the tubule represented as a sheer drop. In a real sample, the lumen wall is sloped so this boundary effect should be not be as significant. In any event, the fluctuations across the cross-section of the PTD are much smaller than those observed experimentally, and indicate that the reason for the observed gradient in hardness is not a boundary effect, but represents a real gradation of the sample material properties across the PDT cross-section.

Conclusions

AFM-based experiments give clear evidence of a gradient of mechanical properties across the PTD and through the PTD-ITD junction. Although clearly boundary effects must be considered, and will influence the absolute values measured, the results indicate that the PTD undergoes a graded change in hardness/modulus across its cross-section. The BE results indicate an inverse relation between the stiffness and piezoresponse, reflecting the changing ratio of collagen-mineral content near to and across the PIJ, supporting previous analytical work which suggested that such a gradient exists. Quasi-static indentations made at minimal applied load provide a quantitative substantiation of these results through the gradient in hardness measurements. FEA simulations show a small boundary effect should exist (PTD vs. lumen hollow on inner side and PTD vs. ITD at outer bound), but it is much smaller

than that observed experimentally. These results, taken together, indicate that the experimentally-observed gradient in the mechanical properties of the PTD is not an experimental artifact of the nearby boundary, but a true reflection of the local materials properties.

Acknowledgements:

A portion of this research was conducted at the Center for Nanophase Materials Sciences, which is sponsored at Oak Ridge National Laboratory by the Division of Scientific User Facilities, U.S. Department of Energy. We gratefully acknowledge The Weizmann Institute's 2005 Karyn Kupcinet International Science Summer School for hospitality and support of Nathan Apter. Support from the Israel Science Foundation grant No 758/07 and from the historic generosity of the Harold Perlman Family is acknowledged. H.D. Wagner is the Livio Norzi Professor in Materials Science.

Table 1. Hardness values measured by AFM in different parts of the dentin.

Position	Lumen edge	Between lumen and mid-PTD	Between mid-PTD and PIJ	Within ITD
H(GPa)*	4 ±0.5	4.7 ± 0.8	1.8 ± 0.4	1.2 ± 0.2

*H determined from Eq. 1 with A_c the projected area determined from grain analysis of the indentation footprint giving projected area in the AFM image.

Table 2 – Results of FEA simulations of 50 nm deep indentations at different positions in PTD

Dist. From Lumen (μm)	Dist from PIJ. (μm)	Max. Force (μN)	E* (GPa)	E (GPa)
0.2	1.0	180	28.8	26.7
0.4	0.8	201.5	32.2	29.8
0.6	0.6	203.4	32.8	30.4
0.8	0.4	202.8	33.0	30.6
1.0	0.2	201.2	32.4	30.0
Flat	infinite	226.8	37.8	35

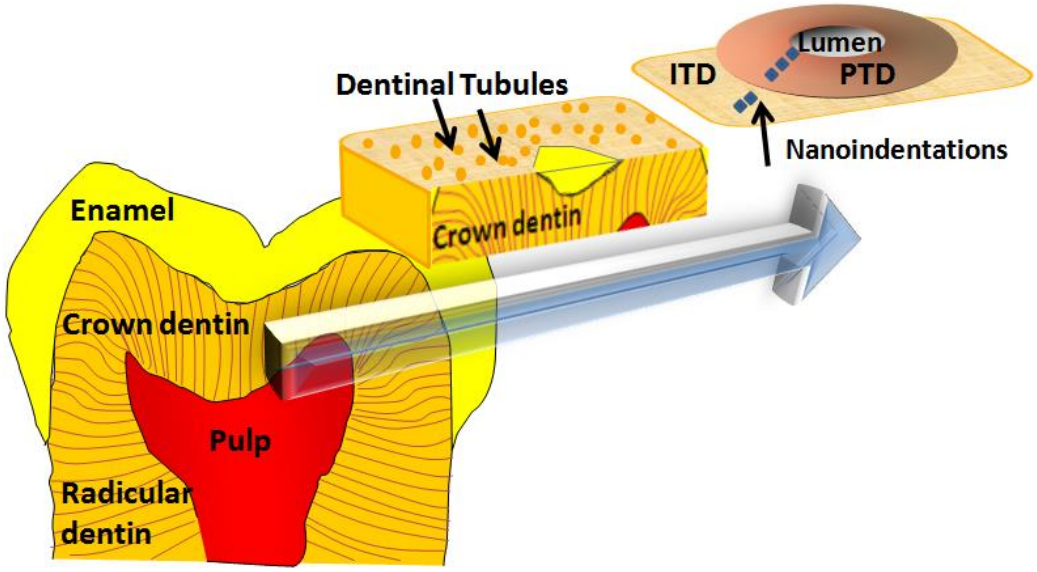

Fig. 1: Schematic presentation of the experimental area in relation to tooth structure at various size scales diminishing in direction of arrow. In rightmost figure, structure of a single tubule is shown with the lumen (inner core) encompassed by the peritubular dentin (PTD), which is further surrounded by the intertubular dentin (ITD)

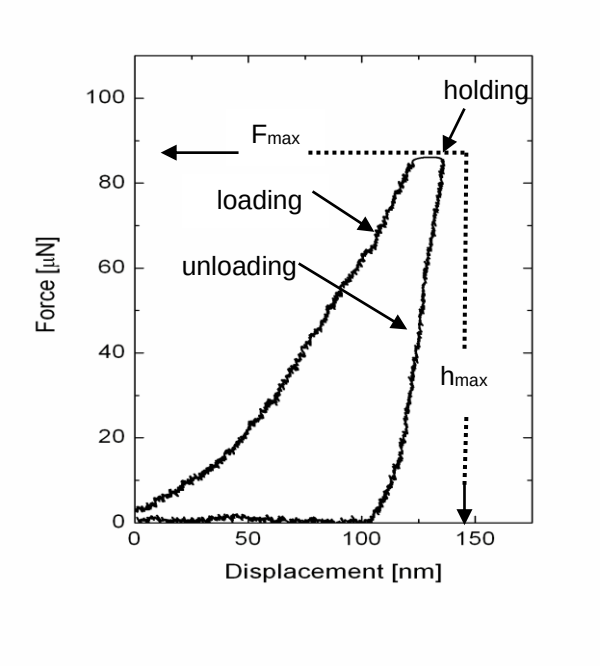

Fig.2 A force-displacement curve obtained during AFM indentation on dentin specimen.

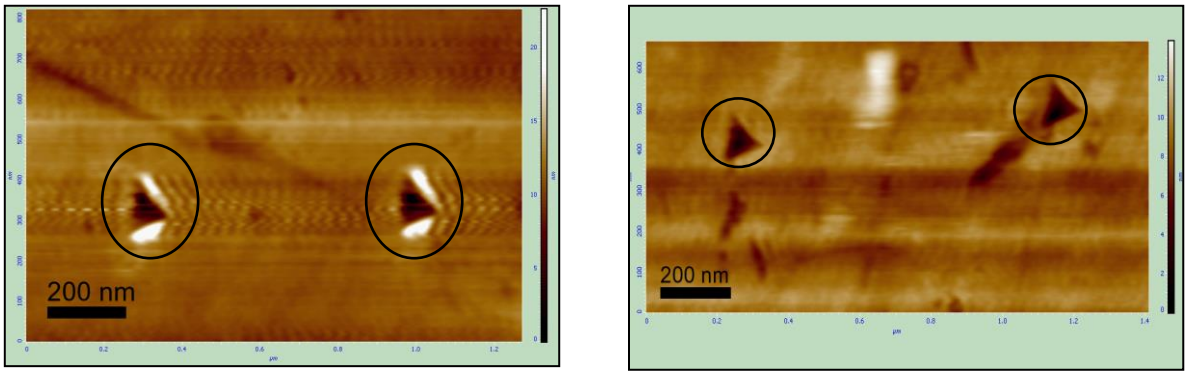

Figure 3 _AFM images of indentations in fused silica with limiting force of 100 μN. Left, example of an approach angle(55º) for which the pile-up was asymmetric. Right side, symmetric indentations are evident in the working approach angle of 35º

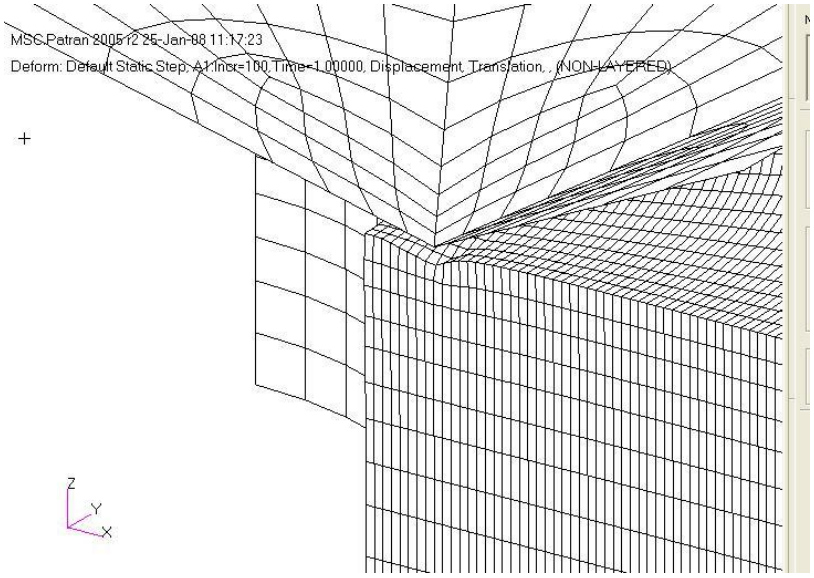

Figure 4 FEA model, showing part of grid under deformation for innermost indent, 0.2 μm from tubular lumen.

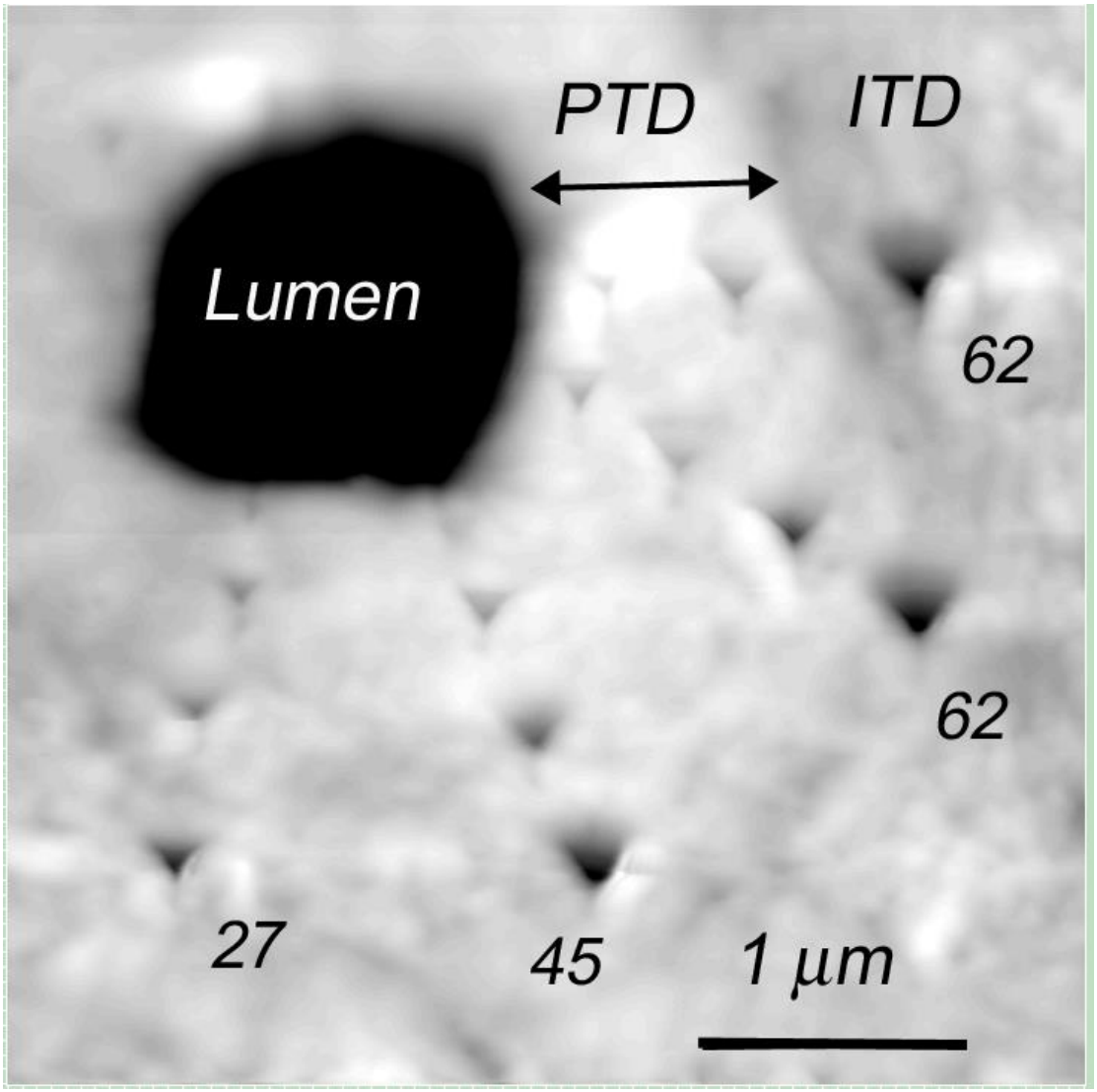

Figure 5 - AFM image of indentations performed on a peritubular dentin along four radial lines, each at constant force using a cube-corner indenter. Maximum load in μN, appears on the figure for each set of indentations. Size of footprint is seen to grow with distance from peritubular lumen. The PTD is seen as the bright ring around the lumen as indicated by annotations in figure. The height greyscale is limited to a range of 200 nm for black-white.

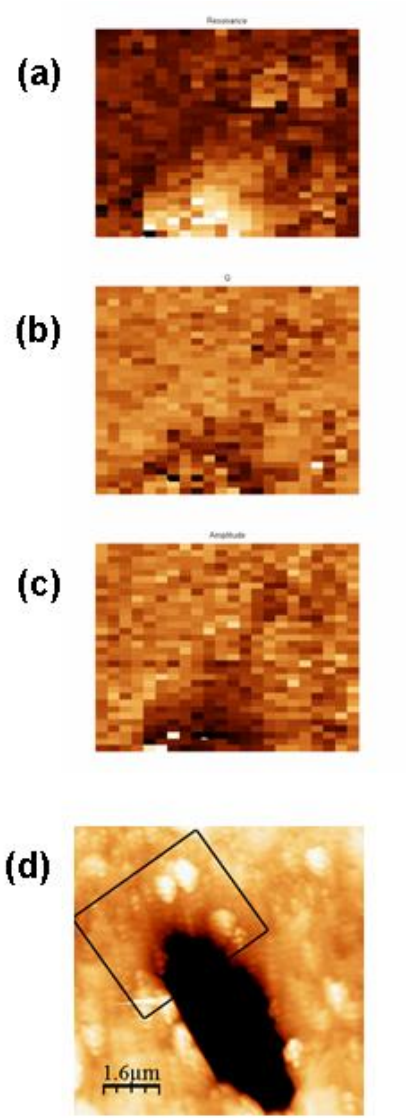

Figure 6 – Frequency (a), dissipation (b), amplitude (c), and topography (d) images of dentin sample. The topography image was made in contact mode, and the BE was driven with electromechanical excitation. Image (d) processed by WSxM software.[31] The rectangle in the topography image is the grid area for the BE images.

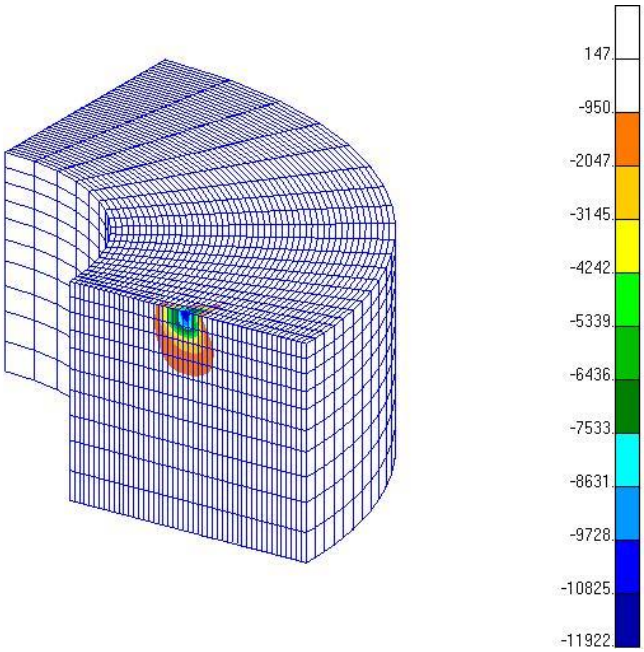

Figure 7 – Result of FEA calculation showing distribution of normal stresses for an indentation 600 nm from the lumen wall at maximum (50 nm) indentation depth.

REFERENCES

[1] Marshall, G.W.; Grayson W.; Marshall, S.J.; Kinney, J.H.; Balooch, M., *J. Dent 1997*., **25**: 441.
[2] Wang, R.; Weiner, S., *Connect Tissue Res* 1998, **39**: 269.
[3] Kinney, J.H.; Marshall,S.J.; Marshall, G.W., Crit Rev Oral Biol Med, 2003. **14**:13.
[4] Mahoney, E.; Holt, A.; Swain, M.; Kilpatrick, N. *J. Dent.* 2000, **28**: 589.
[5]Balooch, G.; Marshall; G.W., Marshall, S.J.; Warren, O.L.; Asif, S.A.; Balooch, M., *J. Biomech.,* **2004, 37**: 1223.
[6] Kinney, J.H.; Balooch, M.; Marshall, S.J.; Marshall, G. W.; Weihs, T.P., *Arch. Oral Biol.*, 1996, **41**: 9.
[7]Balooch, M.; Demos, S.G.; Kinney, J.H.; Marshall, G.W.; Balooch, G.; Marshall, S.J., *J. Mater. Sci. Mater. Med. 2001*, **12**:507.
[8] Doerner, M.F.; Nix, W.D., *J. Mater. Res 1986.*, **1:** 601.
[9] Oliver, W.C.; Pharr, G.M., *J. Mater. Res. 199*2, **7**: 1564. Oliver, W.C. and Pharr, G.M. *J. Mater. Res.,* **19**(1), 3-20, (2004).
[10] Oliver, W.C. and Pharr, G.M. *J. Mater. Res.2004,* **19:** 3.
[11] Burnham, N.A.; Colton, R.J., *J. Vac. Sci. Technol. A* 1989, **7**: 2906.
[12] Vanlandigham, M.R.; Mcknight, S.H.; Palmese, G.R.; Eduljee, R.F.; Gillespie, J.W. Jr,; McCulough, R.L., *J. Mat. Sci. Lett.1997*, **16**:117.
[13] Van Landigham, M, *Microscopy Today* 1997, **97:**12.
[14] P. Maivald, HJ Butt, SAC Gould, CB Prater, B Drake, JA Gurley, VB Elings, and PK Hansma, Nanotechnology 1991, **2** 103.
[15] Yamanaka, K.; Ogiso, H.; Kolosov, O., Appl. Phys. Lett. 1995, **64**:178.
[16] Kester E.; Rabe U; Presmnes L; Tailhades Ph; Arnold W. *J,. Phys. Chem. Solids* 2000, **61**:1275.
[17] Wang, T.;Fenga, Z.; Song Y.; Chen, X.; Dental Materials 2007, **2 3 :** 450.
[18] Habelitz S.; Rodriguez, B.J.; Marshall, S.J.; Marshall, G.W.; Kalinin, S.V.; Gruverman A., J Dent Res 2007, **6**:908.
[19] Turner, J.A.; Hirsekorn, S., Rabe, U.; Arnold, W., *J. Appl. Phys.* 1997, **82**: 966.
[20] Burnham, N.A.; et al, *Nanotechnol.* 1997, **8**:67
[21] Jesse, S.; Kalinin, S.V.; Proksch, R.; Baddorf, A.P.; Rodriguez,B.J., *Nanotechnology2007,* **18**:435503.
[22] Kinney, J.H.; Balooch, M.; Marshall, S.J.; Marshall, G.W.;Weihs, T.P., *J. Biomech. Eng.*, 1996, **118**:133.
[23] Gruverman, A.; Wu, D.; Rodriguez, B.J.; Kalinin, S.V.; Habelitz, S. *Biochemical and Biophysical Research Communications* 2007, **352**: 142.
[24] Habelitz, S.; Marshall, S.J.; Marshall Jr. G.W.; Balooch, M. *J. Struct. Biol.* 2001,**135**: 294.
[25] Kinney, J.H.; Balooch, M. *Arch. Oral Biol*. 1999, **44**:813.
[26] Jakes, J.E.; Frihart, C.R.; Beecher, J.F.; Moon, R.J.; Stone, D.S., *J. Mater. Res.*, 2008 (April, in press).
[27] Qin, Q.H.; Swain, M.V. *Biomaterials*, 2004, **25**: 5081.
[28] Bolshakov, A.; Pharr, G.M., *J. Mater. Res*. 1998, **13**:1049.
[29] Amitay-Sadovsky, E.; Wagner, H.D. *Polymer* 1998, **39**:2387.
[30] Weiner, S.; Veis, A.; Beniash, E.; Arad, T.; Dillon, J. W.; Sabsay, B.; Siddiqui, F., *J. Struct. Biol.*,, 1999 **126**,: 27.
[31]Horcas,I.; Fernandez, R.; Gomez-Rodriguez, J.M.: Colchero, J.; Gomez-Herrero J. ; and Baro, A. M. , *Rev. Sci. Instrum.* 2007 **78**:013705.